

Pressure generation under deformation in a large-volume press

Saisai Wang(王赛赛), Xinyu Zhao(赵鑫宇), Kuo Hu(胡阔), Bingtao Feng(丰丙涛), Xuyuan Hou(侯旭远), Yiming Zhang(张羿鸣), Shucheng Liu(刘书成), Yuchen Shang(尚宇琛), Zhaodong Liu(刘兆东), Mingguang Yao(姚明光), and Bingbing Liu(刘冰冰)

Citation: Chin. Phys. B, 2024, 33 (**9**): 098104. DOI: 10.1088/1674-1056/ad58c6
Journal homepage: http://cpb.iphy.ac.cn; http://iopscience.iop.org/cpb

What follows is a list of articles you may be interested in

Recension of boron nitride phase diagram based on high-pressure and high-temperature experiments

Ruike Zhang(张瑞柯), Ruiang Guo(郭睿昂), Qian Li(李倩), Shuaiqi Li(李帅琦), Haidong Long(龙海东), and Duanwei He(贺端威)

Chin. Phys. B, 2024, 33 (**10**): 108103. DOI: 10.1088/1674-1056/ad6a06

Diamond growth in a high temperature and high pressure Fe-Ni-C-Si system: Effect of synthesis pressure

Yang Liu(刘杨), Zhiwen Wang(王志文), Bowei Li(李博维), Hongyu Zhao(赵洪宇), Shengxue Wang(王胜学), Liangchao Chen(陈良超), Hongan Ma(马红安), and Xiaopeng Jia(贾晓鹏)

Chin. Phys. B, 2023, 32 (**12**): 128102. DOI: 10.1088/1674-1056/acf03d

High-pressure and high-temperature sintering of pure cubic silicon carbide: A study on stress-strain and densification

Jin-Xin Liu(刘金鑫), Fang Peng(彭放), Guo-Long Ma(马国龙), Wen-Jia Liang(梁文嘉), Rui-Qi He(何瑞琦), Shi-Xue Guan(管诗雪), Yue Tang(唐越), and Xiao-Jun Xiang(向晓君)

Chin. Phys. B, 2023, 32 (**9**): 098101. DOI: 10.1088/1674-1056/aca6d4

Effect of the codoping of N—H—O on the growth characteristics and defects of diamonds under high temperature and high pressure

Zhenghao Cai(蔡正浩), Bowei Li(李博维), Liangchao Chen(陈良超), Zhiwen Wang(王志文), Shuai Fang(房帅), Yongkui Wang(王永奎), Hongan Ma(马红安), and Xiaopeng Jia(贾晓鹏)

Chin. Phys. B, 2022, 31 (**10**): 108104. DOI: 10.1088/1674-1056/ac7866

Synthesis and characterizations of boron and nitrogen co-doped high pressure and high temperature large single-crystal diamonds with increased mobility

Xin-Yuan Miao(苗辛原), Hong-An Ma(马红安), Zhuang-Fei Zhang(张壮飞), Liang-Chao Chen(陈良超), Li-Juan Zhou(周丽娟), Min-Si Li(李敏斯), and Xiao-Peng Jia(贾晓鹏)

Chin. Phys. B, 2021, 30 (**6**): 068102. DOI: 10.1088/1674-1056/abf12c

---

Pressure generation under deformation in a large-volume press

Saisai Wang(王赛赛)[1,†], Xinyu Zhao(赵鑫宇)[1,†], Kuo Hu(胡阔)[1,‡], Bingtao Feng(丰丙涛)[1], Xuyuan Hou(侯旭远)[1], Yiming Zhang(张羿鸣)[1], Shucheng Liu(刘书成)[1], Yuchen Shang(尚宇琛)[1,§], Zhaodong Liu(刘兆东)[1,2,¶], Mingguang Yao(姚明光)[1], and Bingbing Liu(刘冰冰)[1]

[1] *State Key Laboratory of Superhard Materials, Synergetic Extreme Condition User Facility, College of Physics, Jilin University, Changchun* 130012, *China*

[2] *College of Earth Sciences, Jilin University, Changchun* 130012, *China*

(Received 18 April 2024; revised manuscript received 6 June 2024; accepted manuscript online 17 June 2024)

Deformation can change the transition pathway of materials under high pressure, thus significantly affects physical and chemical properties of matters. However, accurate pressure calibration under deformation is challenging and thereby causes relatively large pressure uncertainties in deformation experiments, resulting in the synthesis of complex multiphase materials. Here, pressure generations of three types of deformation assemblies were well calibrated in a Walker-type large-volume press (LVP) by electrical resistance measurements combined with finite element simulations (FESs). Hard Al_2O_3 or diamond pistons in shear and uniaxial deformation assemblies significantly increase the efficiency of pressure generation compared with the conventional quasi-hydrostatic assembly. The uniaxial deformation assembly using flat diamond pistons possesses the highest efficiency in these deformation assemblies. This finding is further confirmed by stress distribution analysis based on FESs. With this deformation assembly, we found shear can effectively promote the transformation of C_{60} into diamond under high pressure and realized the synthesis of phase-pure diamond at relatively moderate pressure and temperature conditions. The present developed techniques will help improve pressure efficiencies in LVP and explore the new physical and chemical properties of materials under deformation in both science and technology.

Keywords: shear/uniaxial deformation, pressure calibration, finite element simulations, large-volume press, high pressure

PACS: 81.40.Lm, 07.35.+k, 62.50.–p, 81.40.Vw **DOI:** 10.1088/1674-1056/ad58c6

1. Introduction

Deformation such as shear and uniaxial compressions can change transition pathway of materials under high pressure, thus significantly affecting the physical and chemical properties of materials.[1–5] A typical example is fullerenes and graphite are extremely stable under hydrostatic pressure at room temperature, but could transform into diamond when large shear stress was applied.[1,2] Study on the transformation of minerals under high pressure with shear deformation also helps understanding of mineral rheology and thereby mass transport processes of the Earth's interior.[6,7]

Deformation at high pressure has been realized in non-hydrostatic devices such as the rotational diamond anvil cell, Rotational–Drickamer, and D-DIA apparatus.[8–12] It can also be generated via a simple shear geometry in an octahedral assembly in the most common and user-friendly Kawai-type and Walker-type large-volume press (LVP), which are used to create hydrostatic pressures. Precise pressure generation upon deformation can only be conducted in those apparatus when combined with *in-situ* synchrotron radiation or acoustic travel-time method.[13,14] Most deformation experiments under high pressure for in-house laboratories are generally based on pressure calibrations derived from those under quasi-hydrostatic conditions.[15,16] Consequently, the effect of deformation on pressure generation is often ignored for in-house LVP experiments. This oversight leads to relatively large pressure uncertainties in high-pressure in-house deformation experiments, thereby always resulting in the synthesis of complex multiphase materials. It also keeps unclear about pressure generation owing to applied different stress distributions in different types of deformation. Therefore, it hinders us to precisely study the variations of physical and rheological properties of materials such as phase transition, creep strength, and crystallographic preferred orientation induced by deformation at high pressures.[6,7,15–22]

In this study, pressure generations under a simple shear and uniaxial deformation were conducted in a Walker-type LVP by using the Al_2O_3/diamond pistons coated with copper/molybdenum thin films. The electrical conductance of the hard pistons in these assemblies enables the detection of resistance discontinuities associated with pressure standard phase transitions. As a result, we can investigate the efficiency of three types of deformation cell assemblies upon compression in LVP. Finite element simulations (FESs) were further em-

[†]These authors contributed equally to this work.
[‡]Corresponding author. E-mail: hukuo@jlu.edu.cn
[§]Corresponding author. E-mail: shangyc@jlu.edu.cn
[¶]Corresponding author. E-mail: liu_zhaodong@jlu.edu.cn

© 2024 Chinese Physical Society and IOP Publishing Ltd

ployed to analyze the stress distribution within these deformation cell assemblies, thereby constraining pressure behavior in the LVP. Finally, the effect of deformation on phase transition from C_{60} to diamond is discussed based on our developed techniques.

2. Experiment methods

In our study, high pressure experiments were conducted using tungsten carbide (WC) anvils in the JLUHC-1000 Walker-type LVP with a maximum load of 10 MN. More detailed information of this LVP can refer to our previous study.[23] Eight inner second-stage WC anvils produced by Chengdu Jinwu Hardsteel Carbide Co. LTD., specifically named HXR, were used for generating high pressure. These anvils have an edge length of 25.4 mm and a truncated edge length (TEL) of 5 mm. The Vickers hardness of these anvils is about 18.3 GPa (see Fig. S1(a) of supporting information). Semi-sintered CoO-doped (10 wt%) MgO octahedron (Vickers hardness: 0.6 GPa) was used as the pressure medium. Materials of molybdenum (Mo) and hard Al_2O_3/diamond were used as the pistons for quasi-hydrostatic and deformation high-pressure assembly, respectively.

Quasi-hydrostatic pressure calibration experiments were conducted by using a conventional 10/5 assembly equipped with Mo rods as electrodes. The Vickers hardness of the Mo rods is 3.2 GPa, as shown in Fig. S1(b) of the supporting information, which is not much different from that of the CoO-doped MgO pressure medium (Fig. 1(a)). Samples with a height of $\sim$ 1 mm were loaded into the cell and placed between the upper and lower Mo electrodes. For the shear deformation assemblies (SDAs) used in pressure calibration, dense Al_2O_3 or diamond rods were employed as pistons. Their Vickers hardness values are approximately 14.1 GPa and 128 GPa, respectively (Figs. S1(b)–S1(d)), which are much harder than the MgO pressure medium. Shear deformation under compression is induced by adopting 45° slanted Al_2O_3 and diamond as pistons, the schematic diagram is shown in Fig. 1(b). Additionally, flat diamond pistons with a height of 1.0 mm were adopted as the pistons in the uniaxial deformation assembly (UDA) (Fig. 1(c)). Pressures generated using these newly designed assemblies are compared by detecting the electrical resistance changes associated with the I–II (6.6 GPa), II–III (8.9 GPa), and III–IV (12.9 GPa) phase transitions of ZnTe and semiconductor–metal transitions of ZnS (15.6 GPa).

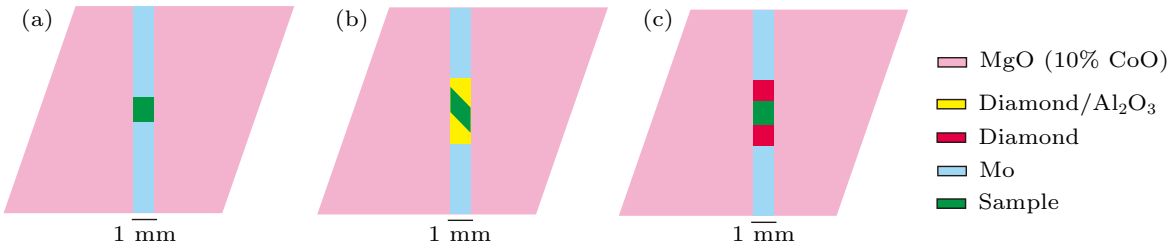


Fig. 1. Schematic diagram of conventional quasi-hydrostatic assembly (QHA) with Mo rods (a), shear deformation assemblies with 45° slanted Al_2O_3/diamond pistons (b), and uniaxial deformation assembly with flat diamond pistons (c).

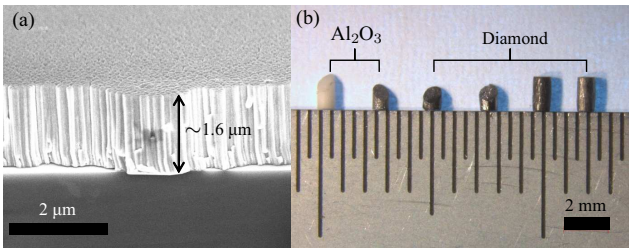


Fig. 2. Micrographs of Cu plated on a silicon sheet, which is corresponding to the thickness of Cu plated on Al_2O_3/diamond pistons (a). 45° slanted Al_2O_3/diamond and flat diamond pistons before and after coating metal thin films (b).

To realize the resistance measurement of pressure standards in the deformation assemblies, thin Cu or Mo films were deposited on the entire surfaces of the hard alumina and diamond pistons by using the magnetron sputtering method. The sputtering power, time, and heating temperature are about 100 W, 10 min, and 600 K respectively. During the deposition process, a silicon sheet was placed together with the Al_2O_3 and diamond pistons. This allowed us to directly observe the thickness of the Cu or Mo thin film on the silicon sheet, which was identical to that on the Al_2O_3 and diamond pistons. Scanning electron microscope (SEM) observation shows that the thickness of these films was approximately 1.6 μm (Fig. 2(a)). Such a thin metal film can make diamond and Al_2O_3 pistons electroconductive without losing its macroscopic mechanical properties, enabling the detection of sample resistance during compression in the Walker-type LVP. This approach ensures accurate resistance measurements even under high pressure conditions.

FESs were performed by using a commercial software OPTISTRUCT, which showed the stress distribution in the octahedron under compression. Figure 3 shows the designed octahedron models for calculation, in which the mesh size is 0.1 mm. Table S1 summarizes the mechanical property parameters of materials employed in the simulation. In addition, to simplify the model, a metal cylinder made of aluminum (Al) was used as the sample. During simulation the same load was exerted on each equilateral triangular face of the octahedron, consistent with actual experiments.

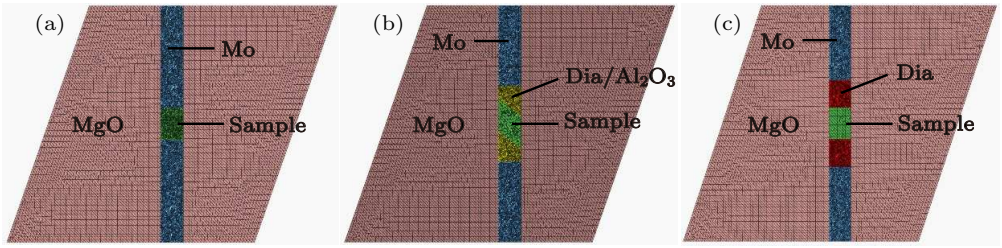


Fig. 3. FESs models for QHA (a), SDAs with Al_2O_3/diamond (b), and UDA (c).

The C_{60} samples recovered from the HPHT experiments were polished with a diamond grinding disc, and then ultrasonically cleaned with acetone for half an hour. The phase composition of the samples was identified using an x-ray diffractometer (R-AXIS RAPID II, Rigaku, Japan) with Cu $K\alpha$ radiation (wavelength, 1.5418 Å) at 40 kV and 30 mA.

3. Results and discussion

Coating Cu or Mo on the entire surfaces of Al_2O_3 or diamond pistons allows for precise detection of resistance variations using the deformed assemblies. Pressure generation efficiency in the four cell assemblies were compared by exploiting the phase transitions of ZnTe and ZnS associated with variations in electrical resistance. Figure 4(a) illustrates the electrical resistance changes of ZnTe upon compression in the assemblies using Mo, slanted Al_2O_3/diamond pistons, and flat diamond pistons as electrodes. Compared with quasi-hydrostatic pressure, the phase transition pressure point of ZnTe does not change significantly under non-hydrostatic pressure.[24] As is seen, the corresponding press loads of three deformation assemblies at the three phase transitions (I–II: 6.6 GPa, II-III: 9.9 GPa, III–IV: 12.9 GPa) of ZnTe using diamond and Al_2O_3 pistons are significantly lower than those of QHA using Mo rods, indicating the higher efficiency of pressure generation for the deformation assemblies. It is found that applied press load corresponding to the first and second phase transitions for the deformation assembly using diamond pistons is comparable to that using Al_2O_3 pistons. However, the third phase transition by the former is slower than the latter, and is much faster than those using Mo pistons. It could be due to the higher hardness of diamond compared to that of Al_2O_3.

The resistance changes of ZnS with press load for these assemblies are shown in Fig. 4(b). A sharp decrease of the electrical resistance can be observed when the phase transition of ZnS occurs upon the applied press load for all assemblies, which corresponds to a pressure of 15.6 GPa. Specifically, the applied press load on the UDA with flat diamond pistons for this phase transition is 3.64 MN. This value is significantly lower than that observed for the SDAs with slanted Al_2O_3 (4.31 MN) and diamond (4.53 MN). All these three deformation assemblies possess a relatively lower press load than that of the conventional quasi-hydrostatic assemblies (5.11 MN).

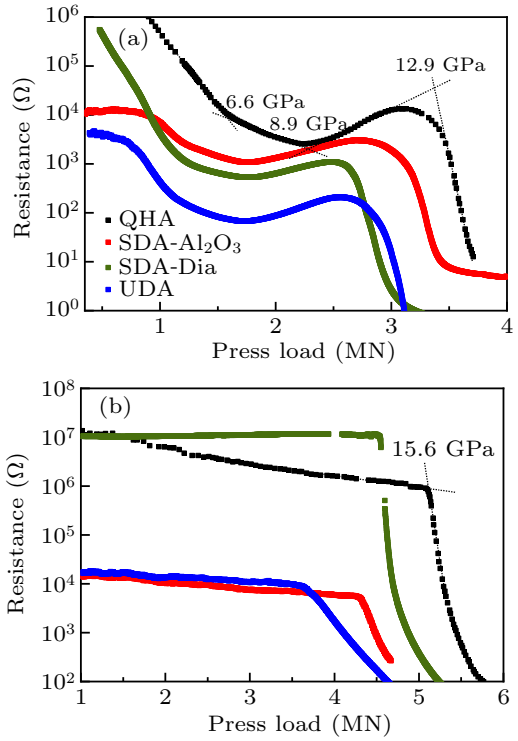


Fig. 4. Variations of electrical resistance upon compression for the pressure standard materials ZnTe (a) and ZnS (b) using QHA and S/UDAs, respectively.

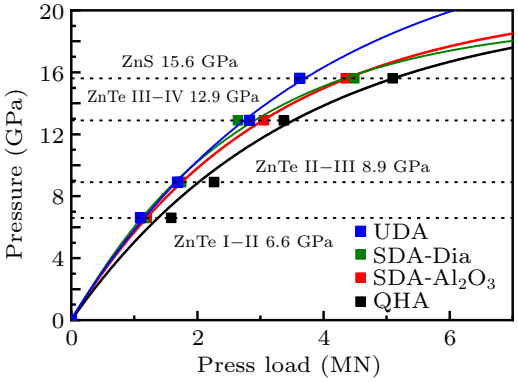


Fig. 5. Pressure generation of four types of 10/5 assemblies at room temperature using HXR WC anvils in Walker-type LVP.

The sample pressure for the three deformation assemblies and one QHA assembly was well calibrated against the applied press load at room temperature. As shown in Fig. 5, the press loads corresponding to phase transition of standard material for the QHA are always higher than that for deformation assemblies, demonstrating that the deformation assemblies have higher efficiency in pressure generation. This observation can

be attributed to the higher hardness of Al_2O_3 and diamond relative to Mo and (Mg, Co)O materials. For the three deformation assemblies, they also exhibit different efficiency of pressure generation. Below 12.9 GPa, the efficiency of pressure generation in deformation assemblies with flat diamond pistons is comparable to that achieved with 45° slanted diamond and Al_2O_3 pistons. However, when the pressure exceeds 12.9 GPa, the efficiency of pressure generation using UDA significantly exceeds that achieved with SDA. This is due to part of the pressure are decomposed into the direction parallel to the oblique plane in SDA, which also generates a strong shear stress field in the sample. One representative back-scattering electron image shows that the pressure marker of ZnS is well sandwiched by the 45° slanted diamond pistons as shown in Fig. S2 of the supporting information.

To understand how the shape and hardness of pistons affect the efficiency of pressure generation in these assemblies, we performed FESs, which showed the stress distribution in the octahedron under compression. Figure 6 presents the stress distribution contour maps for various assemblies under a constant load of 4 MN, as obtained from FESs. The black markings in the figure correspond to the lowest pressure within the sample areas. It was clearly found that the sample pressure derived from the three deformation assemblies exceeds that of the QHA, consistent with the experimental findings shown in Fig. 5. Note that the UDA assembly with flat diamond pistons result in the most concentrated stress distribution at the assembly's center, consequently yielding the highest pressure among these assemblies. All these above simulation results well support our experimental findings as shown in Fig. 5.

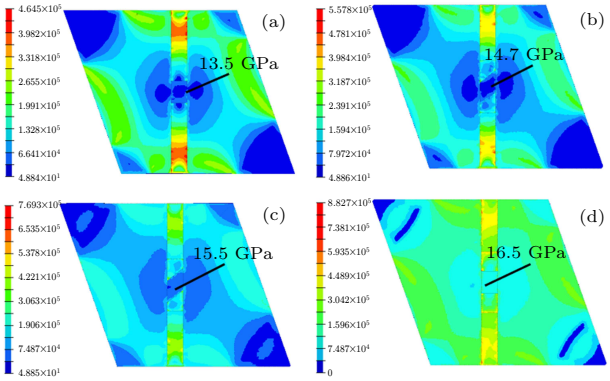


Fig. 6. Stress distribution contour maps for the QHA (a), SDA-Al_2O_3 (b), SDA-Dia (c), and UDA (d), respectively.

The deformation assembly was applied in the HPHT experiments through properly designing internal structures in conventional 10/5 assemblies. Figure S3 shows the designed deformation assembly, in which the starting material was loaded into an MgO sleeve and placed between two upper and lower 45° slanted diamond pistons, thermocouples were directly connected to the center of the wall of the cylindrical rhenium heater. Figure S4 shows the heating performance of the SDA that can stably generate high temperature above 1300 K at high pressure, and the heating efficiency is higher than that of QHA. Relies on the deformation and conventional cell assemblies, we conducted four HPHT experiments at a pressure range of 14 GPa–18 GPa and a temperature range of 1273 K–1673 K, studying the effect of shear deformation on the phase transition of C_{60} to diamond.

Figure 7 shows the x-ray diffraction (XRD) characterization of the recovered samples. For the two SDA experiments, the XRD patterns both exhibit three distinct diffraction peaks corresponding to the (111), (220), and (311) crystal planes of cubic diamond, suggesting the formation of diamond in these samples. At the press load of 4.62 MN (16 GPa) and 1273 K, C_{60} has completely transformed into a diamond phase, while for the low-pressure experiments (14 GPa) the (002) diffraction peak of graphite was observed in the XRD pattern, suggesting an incomplete transformation of C_{60}. However, for the quasi-hydrostatic pressure experiments using QHA, the XRD results shows C_{60} transformed to compressed graphite and amorphous carbon at a press load of 4.71 MN (15 GPa) under 1273 K and the formation of diamond need a higher press load of 7.61 MN (18 GPa) and temperature of 1673 K. Referring to the *P*–*T* phase diagram of C_{60} (see Fig. S5),[25–28] the transformation of C_{60} to diamond under quasi-hydrostatic conditions requires reaching approximately 16 GPa and 1560 K. This indicates that shear deformation significantly promotes the phase transition of C_{60} to diamond compared to quasi-hydrostatic experiments. Furthermore, this deformation technology under high pressure enables phase-pure diamond synthesis under low press loads, thereby extending the service life of WC anvils and possessing significant potential for applications in the diamond industry.

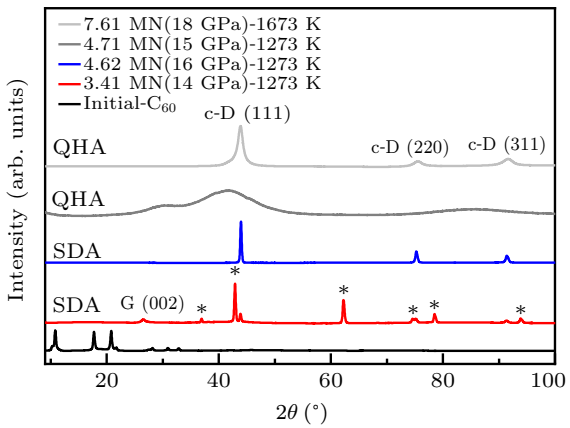


Fig. 7. XRD patterns for samples using SDA and QHA recovered from different high-pressure and high-temperature conditions. The bottom black line is the XRD pattern of C_{60} precursor. Abbreviations G and c-D represent graphite and cubic diamond, respectively. The asterisk comes from the diffraction peak of magnesium oxide inclusions.

4. Conclusion

In this paper, we achieved precise pressure calibrations for several deformation assemblies by coating metal film on diamond or Al_2O_3 pistons using the magnetron sputtering technique in a Walker-type LVP. These metal films on the piston surfaces create an electrically conductive pathway, allowing us to measure resistance changes of pressure standards during the compression process in deformation experiments. It is found that the pressure generation efficiency of SDAs with Al_2O_3/diamond pistons is significantly higher than that of the QHA with Mo rods in LVP. The UDA with flat diamond pistons exhibits the highest efficiency of pressure generation among all the deformation assemblies. These observations are further demonstrated by analyzing the stress distribution within the aforementioned assemblies using FESs. It is found that diamond can be synthesized at a relatively lower temperature and pressure conditions from C_{60} starting material under simple shear deformations compared to conventional quasi-hydrostatic conditions. Pressure generation of in-house simple shear and uniaxial deformation experiments are clarified using the present technique. It will enhance our understanding of phase transitions under shear deformations and facilitate further exploration of the physical and chemical properties of materials.

Acknowledgements

We acknowledge Yankun Yin for SEM analysis. Project supported by the National Natural Science Foundation of China (Grant Nos. 42272041, 41902034, 52302043, 12304015, 52302043, and 12011530063), the National Major Science Facility Synergetic Extreme Condition User Facility Achievement Transformation Platform Construction (Grant No. 2021FGWCXNLJSKJ01), the China Postdoctoral Science Foundation (Grant Nos. 2022M720054 and 2023T160257), the National Key Research and Development Program of China (Grant No. 2022YFB3706602), and the Jilin University High-level Innovation Team Foundation, China (Grant No. 2021TD–05).

References

[1] Regueiro M N, Monceau P and Hodeau J L 1992 *Nature* **355** 237
[2] Dong J J, Yao Z, Yao M G, Li R, Hu K, Zhu L Y, Wang Y, Sun H H, Sundqvist B, Yang K and Liu B B 2020 *Phys. Rev. Lett.* **124** 065701
[3] Serebryanaya N R, Blank V D, Ivdenko V A and Chernozatonskii L A 2001 *Solid State Commun.* **118** 183
[4] Gao Y, Ma Y Z, An Q, Levitas V, Zhang Y Y, Feng B, Chaudhuri J and Goddard W A 2019 *Carbon* **146** 364
[5] Tyukalova E, Kulnitskiy B, Perezhogin I, Kirichenko A and Blank V In Society EM ed. *European Microscopy Congress* 2016: *Proceedings Weinheim* (Germany: Wiley-VCH Verlag GmbH & Co. KGaA 2016 303)
[6] Zhang S Q, Karato S, Fitz Gerald J, Faul U H and Zhou Y 2000 *Tectonophysics* **316** 133
[7] Karato S, Zhang S Q and Wenk H R 1995 *Science* **270** 458
[8] Levitas V I, Ma Y Z, Hashemi J, Holtz M and Guven N 2006 *J. Chem. Phys.* **125** 044507
[9] Kawazoe T, Karato S, Otsuka K, Jing Z C and Mookherjee M 2009 *Physics of the Earth and Planetary Interiors* **174** 128
[10] Wang Y B, Durham W B, Getting I C and Weidner D J 2003 *Rev. Sci. Instrum.* **74** 3002
[11] Nishiyama N, Wang Y B, Sanehira T, Irifune T and Rivers M 2008 *High Pressure Res.* **28** 307
[12] Ohuchi T, Kawazoe T, Nishiyama N, Yu N and Irifune T 2010 *J. Earth Sci.* **21** 523
[13] Li L B 2018 *Chin. J. Polym. Sci.* **36** 1093
[14] Ves S, Schwarz U, Christensen N E, Syassen K and Cardona M 1990 *Phys. Rev. B* **42** 9113
[15] Wang L, Blaha S, Kawazoe T, Miyajima N and Katsura T 2017 *Geophys. Res. Lett.* **44** 2687
[16] Wang L, Blaha S, Pintér Z, Farla R, Kawazoe T, Miyajima N, Michibayashi K and Katsura T 2016 *Earth and Planetary Science Letters* **441** 81
[17] Karato S and Rubie D C 1997 *J. Geophys. Res.* **102** 20111
[18] Wang L, Chanyshev A, Miyajima N, Kawazoe T, Blaha S, Chang J and Katsura T 2022 *Earth and Planetary Science Letters* **579** 117360
[19] Wang L, Miyajima N, Kawazoe T and Katsura T 2019 *American Mineralogist* **104** 47
[20] Demouchy S, Tommasi A, Barou F, Mainprice D and Cordier P 2012 *Physics of the Earth and Planetary Interiors* **202–203** 56
[21] Katayama I and Karato S 2008 *Physics of the Earth and Planetary Interiors* **168** 125
[22] Holtzman B K, Groebner N J, Zimmerman M E, Ginsberg S B and Kohlstedt D L 2003 *Geochem. Geophys. Geosyst.* **4** 8607
[23] Shang Y C, Shen F R, Hou X Y, Chen L Y, Hu K, Li X, Liu R, Tao Q, Zhu P W, Liu Z D, Yao M G, Zhou Q, Cui T and Liu B B 2020 *Chin. Phys. Lett.* **37** 080701
[24] Zhuang Y K, Dai L D, Li H P, Hu H Y, Liu K X, Yang L F, Pu C and Hong M 2018 *Mod. Phys. Lett. B* **32** 1850342
[25] Shang Y C, Liu Z D, Dong J J, Yao M G, Yang Z X, Li Q Q, Zhai C G, Shen F R, Hou X Y, Wang L, Zhang N Q, Zhang W, Fu R, Ji J F, Zhang X M, Lin H, Fei Y W, Sundqvist B, Wang W H and Liu B B 2021 *Nature* **599** 599
[26] Horikawa T, Suito K, Kobayashi M and Onodera A 2001 *Phys. Lett. A* **287** 143
[27] Wood R A, Lewis M H, Bennington S M, Cain M G, Kitamura N and Fukumi A K 2002 *J. Phys.: Condens. Matter* **14** 11615
[28] Brazhkin V V and Lyapin A G 2012 *J. Superhard Mater.* **34** 400